Effects of Bio-Inspired Surface Roughness on a Swept Back Tapered NACA 4412 Wing

Khurshid Malik[1], Mohammed Aldheeb[1], Waqar Asrar[1,*], Sulaeman Erwin[1]

Malik K https://orcid.org/0000-0001-5054-8056

Aldheeb M https://orcid.org/0000-0002-8270-8373

Asrar W https://orcid.org/0000-0003-2896-0284

Erwin S https://orcid.org/0000-0003-1584-6271

ABSTRACT: This paper presents the overall pros and cons of the effect of surface roughness elements over a NACA 4412 tapered, swept back half wing with a sweep angle of 30° and a dihedral angle of 5°. The tests were conducted at a Reynolds number of 4×10^5 in the IIUM Low Speed wind tunnel. Different roughness sizes and roughness locations were tested for a range of angle of attack. Lift, drag and pitching moment coefficients were measured for the smooth wing and with roughness elements. Surface roughness delays the stall angle and decreases the lift. The wing with the roughness elements located at 75% to 95% of mean chord from leading edge shows minimum drag and maximum lift compared to other locations. Significant increase in the pitching moment coefficient was found for flexible roughness elements. In case of rigid surface roughness, the effect on pitching moment is small.

KEYWORDS: 3D wing aerodynamic coefficients, Bio-inspired roughness elements, NACA 4412.

INTRODUCTION

The wing surface of birds does not follow a single smooth curve surface. The construction of the body surface of mammals which fly or swim in the water reduces the drag by change in boundary layer dynamics over the surface area of their body (Bechert *et al.* 2000). Reduction of the drag force depends on the Reynolds number (Re). The swift bird flies at low Reynolds number (Re), and its rough wings can produce laminar flow due to the flow traveling more distance from leading edge to trailing edge to produce turbulent flow. The transition of flow allows surprising degrees of independence at the level of surface construction (Lentink and de Kat 2014). Therefore small birds, e.g. swallows and swifts, can have thicker bugging out rachis (which is stronger and stiffer), without affecting aerodynamic properties. This aerodynamic role at low Reynolds numbers might have provided small birds a window to produce laminar flow and glide well, regardless of their basic wing surface construction. It can be used in the design of swift-sized micro air vehicles (MAVs) in which the efficiency does not depend on the smooth surface and the high-Reynolds-number (Laursen 2008).

From an aerodynamic perspective, bird wings have flexible several sequential rows of covering feathers on their wings. The self-activated movable flap helps to develop the lift and it is proven by experiment on an artificial feather of wing that lift can be increased by them. A small number of feathers are positioned in front of the wing's leading edge when birds land and they help to reduce drag on the bird's wing (Bechert *et al.* 2000). Birds provide the motivation for airplane design and early developments

of wing design. However, the air-vehicle does not flap their wing like birds do to produce thrust and lift because it is not practical in air-vehicles due to limitations of high speed and scaling phenomena (Jakab 1990).

Mechanical performance of wings depends on a different type of function and morphology of feathers. The outer primary types of feather are more resistant to aerodynamic force than inner primary feathers, in particular at the tip and the outermost primary feathers of wing act as a reversible airfoil during take-off (Ennos *et al.* 1995). Bird's wing feathers, especially at tip, reduce the drag by allowing air to pass through feathers and use tip reversal upstrokes (Crandell and Tobalske 2011).

An experimental study on rough wing (3D printed swift hand wing) and smooth wing models was conducted using PIV (particle image velocimetry) and force measurements in wind tunnel at Reynolds number from 13,300 to 30,000. The rough model was based on actual dimensions of the fully extended swift wing and compared with a smooth one. The results of the experiment showed that the aerodynamics of the rough swift wing can improve. Swift wing roughness can make a boundary layer laminar at low Reynolds number and low angle of attack. In addition to this, there is little effect on drag and lift to drag ratio (van Bokhorst *et al.* 2015).

The swift bird wing prototype (rough wing) model was investigated in a wind tunnel at Reynolds number between 12,000 to 67,000. The result of the experiment showed that 69% of the wing has laminar flow. Results indicated that drag declined and laminar flow reduced the drag at speeds at which the swift flies (Lentink and de Kat 2014).

Carruthers *et al.* (2010) analyzed the aerodynamic performance of a reconstructed eagle wing 2D airfoil at Reynolds number range from 1×10^5 to 2×10^5 and found that drag is almost fixed over a range of C_L. On the other hand, Withers (1981) said bird wings have a low lift to drag ratio due to high drag coefficient as tested for a dried wing of a bird at Reynolds number 1.5×10^5. Bird wings have low efficiency and they do not perform as well as conventional airfoils (Carruthers *et al.* 2010; Withers 1981). Although they compared wing sections of the bird at low Reynolds number and airfoil at high Reynolds number, which do question mark on this comparison. However, wings of birds have the ability to perform at many ranges of angles of attack (Carruthers *et al.* 2010). Klän *et al.* (2009) investigated two elements, one barn owl geometry based rectangular wing and second modified surface of the wing by velvet using PIV, oil flow pattern and pressure tab technique. The result found that modified element reduced separation on the suction side of the wing at high Reynolds number and moderate angles of attack (Klän *et al.* 2009).

A hairy surface modified flat plate was investigated for its ability to reduce drag (Bartenwerfer and Bechert 1991). Riblet effect on wing surface was also studied and confirmed its ability of reducing skin friction and drag (Schlichting *et al.* 1955; Shyy *et al.* 2013; White and Corfield 1991). It shows that when distributed roughness is applied to the trailing edge over the upper surface of the airfoil, maximum lift coefficient is not greatly reduced until the front edge of the roughness extends forward of 0.1 chord, stage at which also the drag increment becomes much larger due to the roughness rapidly (Gregory and O'Reilly 1973).

The effect of roughness bump over SD7003 rectangular wing at angle of attack α = 2°, 4° and 6° at a low Reynolds number of 60,000 using a numerical method, was examined by Zhou and Wang (2011). The study was based on bump size, location the number of bumps at a different angle of attack. The authors located roughness bump near the leading edge of the wing. The pressure drag forces were reduced when the laminar separation bubbles (LSB) were diminished or avoided, resulting in much-improved lift over drag ratio.

Chakroun *et al.* (2004) conducted a study with several types of roughness elements based on size and location on a NACA 0012 airfoil at a Reynolds number of 1.5×10^5. The authors measured velocity profile, lift, drag, and pressure coefficient. The result indicated that as roughness size increases, lift declines and C_{Dmin} also rises because of increased skin friction.

Chen *et al.* (2016) conducted a CFD and experimental study on diverse types of equivalent particle roughness elements over NACA 4418 airfoil at 0.4×10^6 Reynolds number. They concluded that there was aerodynamics performance decrement as roughness size increased at 10% chord length. On the other hand, aerodynamic performance improved when the roughness size was equal or less than 0.7 mm near the trailing edge.

Almost all the studies performed on surface roughness effects have been made on airfoils. The aim of the present work is to study the effect of surface roughness on a very realistic wing such as a NACA 4412 tapered, swept back half wing with a sweep angle of 30° and a dihedral angle of 5° at the moderate Reynolds number of 4×10^5.

The study on the aerodynamics of roughness effect on the airfoil/wing is important to aviation, since changing the roughness size and location will affect the lift and drag coefficients and hence, the airfoil/wing lifting efficiency. Also, it will affect the stall angle, which is a very important factor for the aerodynamic characteristics. Roughness on the surface may come from natural incidences (ice, snow and frost), pitting produced by sand storms, natural flyer or from a long time in service.

Aerodynamic drag reduction is a key goal for future wing design. The study on effects of surface roughness on a swept back tapered NACA 4412 wing is not available in the literature. This paper discusses the effect of surface roughness elements of different shapes, types (rigid and flexible), and location on the aerodynamic properties of a NACA 4412 swept back tapered half wing.

EXPERIMENTAL SETUP
BASE MODEL DETAIL

In the past, researchers have used several types of airfoil/wing as a base model to study bird wing surface design. In this research, a 3D NACA 4412, tapered (taper ratio 4), 30° sweptback, half-span wing with a dihedral of 5°, is used as the base wing to measure the effect of surface roughness. A six-component force balance in the IIUM LSWT is used for measuring the aerodynamic loads. The base wing description is given in Table 1. Figure 1 shows the drawing of the base wing. The tests were conducted at a Reynolds number of 4×10^5 based on the mean aerodynamic chord.
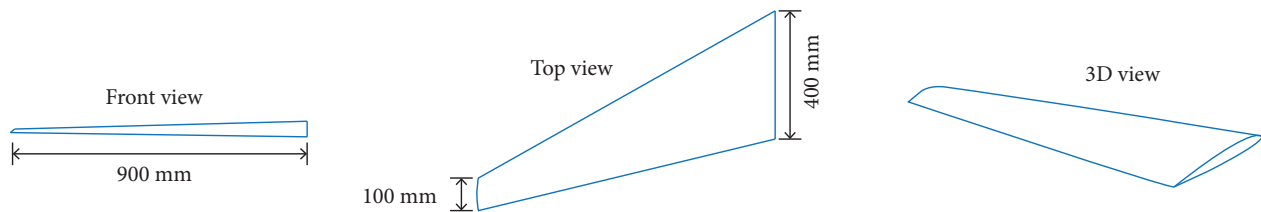

Figure 1. Swept NACA-4412 tapered half wing.

Table 1. Swept NACA 4412 tapered half wing 3D base element.

Model: NACA 4412 wing (taper)		
Type	**Half**	**(Full/half)**
	Wing	
Tip chord (c_t)	0.1	m
Root chord (c_r)	0.4	m
Taper ratio (λ)	4	
Area (A_T)	0.252	m²
Mean chord (c)	0.28	m
Mean geometric chord (c_g)	0.25	m
Span (b)	0.9	m
Swept angle		30°
Dihedral angle		5°
Aspect Ratio		3.6
Reynolds number		4×10^5

ROUGHNESS ELEMENTS

The roughness elements considered for this research are inspired by the bird feather structure. Those specific shapes taken from feather construction (see Fig. 2) were installed on the base wing to analyze its aerodynamics performance in the presence of such roughness elements. Two different types of roughness elements have been considered. In the first case, rigid type of roughness elements have been employed by fixing them on the base wing, restricting any movement whatsoever from wind inside the wind tunnel. Secondly, one specific case of flexible type of roughness element, which can change its orientation during wind tunnel testing, has been used.

Figure 3 shows a description of the location on the NACA 4412 half-span tapered wing. First, the location (A) is taken at 18% to 36% of mean chord (c) from the leading edge (LE) based on the maximum thickness of airfoil, which is 20% of the mean chord (c). Secondly, the location (B), 50% to 70% of mean chord from leading edge, is taken from bird wing of and Eagle, which has major distribution of roughness at 50% to 70% of mean chord from the leading edge. And finally, location (C), 75% to 95% of the mean chord from leading edge, is taken after Chakroun *et al.* (2004), who showed highest lift coefficient up to stall angle at 25% of the airfoil surface and located at the trailing edge (TE).
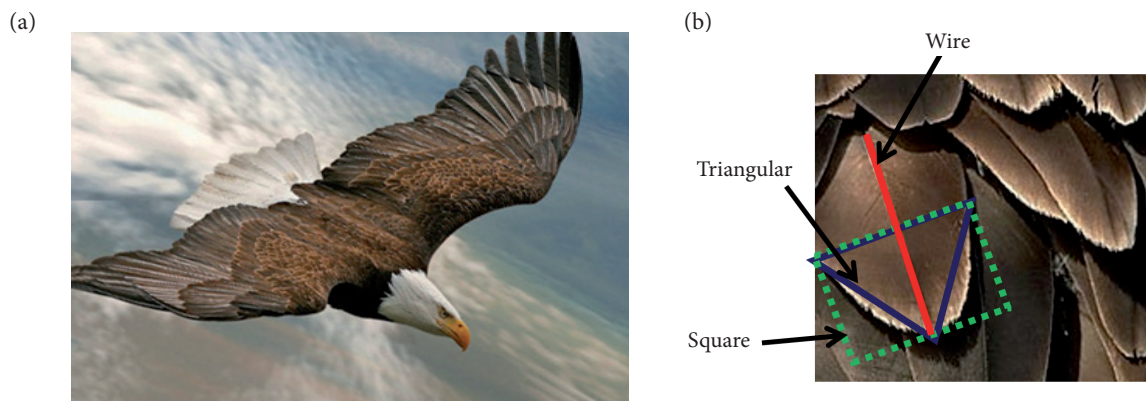
(a) (b)

Figure 2. Roughness elements shape adopted from eagle feather (Hope Rutledge 2018).

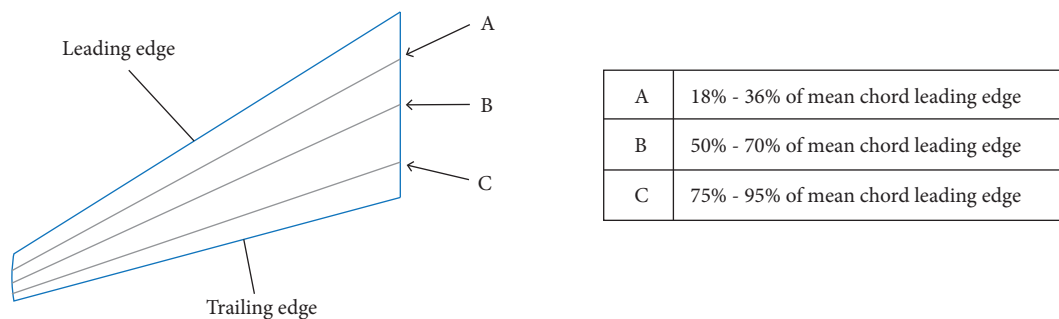| A	18% - 36% of mean chord leading edge
B	50% - 70% of mean chord leading edge
C	75% - 95% of mean chord leading edge

Figure 3. Description of location of roughness on NACA 4412 tapered wing.

In this case, the role of cylindrical (wire) shape is examined by varying the cylindrical diameter at three different locations on the wing. The cylindrical roughness elements (CRE) have three different sizes in diameter of wires, which are 0.5, 1 and 2 mm, to analyze their effect on the NACA 4412 tapered wing. The length of the wire is approximately the same as the base wing. The two wires were fixed to the wing surface using double-sided adhesive tape and super glue to prevent any movement of the wires during testing in the wind tunnel. A black tape was used on both wires for providing enough strength during testing for wind

tunnel. This roughness element was proposed by Chakroun *et al.* (2004), who studied wire elements with 2 mm diameter and 1 cm spacing on a symmetrical NACA 0012 airfoil. The detailed characteristics and dimensions of each type cylindrical roughness elements are given in Table 2.

Table 2. Cylindrical roughness elements description.

S.N.	Element	Element diameter	Element location on wing
1	CRE1	0.5 mm	A
2	CRE2	0.5 mm	B
3	CRE3	0.5 mm	C
4	CRE4	1 mm	A
5	CRE5	1 mm	B
6	CRE6	1 mm	C
7	CRE7	2 mm	A
8	CRE8	2 mm	B
9	CRE9	2 mm	C
Space between two wires for all elements = 1 cm.			

For square roughness element (SRE) of 1 mm thickness, the same three locations A, B and C mentioned earlier were chosen for investigation. This location B was found to be major contributor in the effect on aerodynamic loads. Further a 0.5 mm thick square and a 1 mm thick equal triangular roughness element were investigated at location B. The center-to-center distance between the two elements is 10 mm. Size of all (SREs and TRE) is 5 mm. Table 3 shows the description of SREs and TRE. Figure 4 shows SREs and TRE installation arrangement on wing.

Table 3. Roughness elements (square and triangular) description.

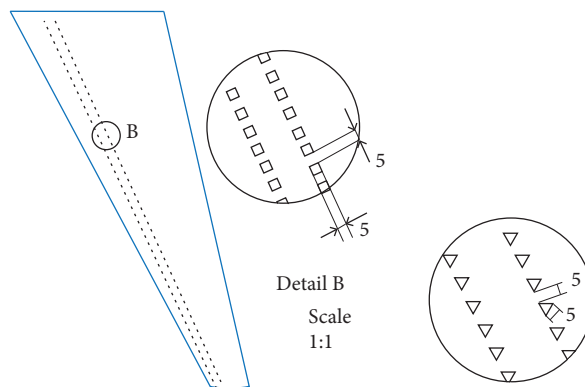| S.N.	Elements	Element type	Element thickness	Element location on wing
1	SRE1	Square	1 mm	A
2	SRE2	Square	1 mm	B
3	SRE3	Square	1 mm	C
4	SRE4	Square	0.5 mm	B
5	TRE	Triangular	1 mm	B

Figure 4. Square and triangular type roughness element at NACA 4412 tapered wing.

The flexible roughness element (FRE) is described in Table 4. The flexible element shape is rectangular and is free to rotate about its transverse end during the test. One end of this flexible rectangular element is fixed on the wing surface by double-sided adhesive tape (see Fig. 5). For FRE, PVC opaque white sheet with 1GPa modulus of elasticity was used to manufacture the elements. This has 0.4 mm thickness and 20 × 14 mm size; the elements are spaced 5 mm apart. Both FREs are same except their different location on the wing, 0.5 c to 0.7 c and 0.7 c to 0.9 c of mean chord from LE mean upper side for FRE1 and FRE2, respectively.

Table 4. Roughness elements (flexible type) description.

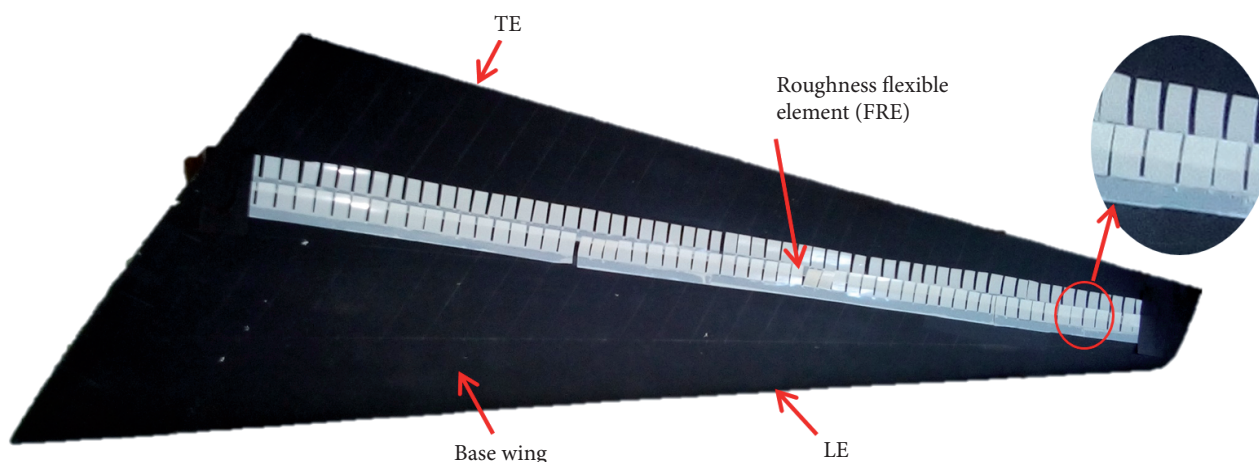| S.N.	Element	Element location on wing
1	FRE1	0.5 c to 0.7 c from LE
2	FRE2	0.7 c to 0.9 c d from LE
Material is PVC opaque white sheet with modulus of elasticity = 1 Gpa		
Size of element = 20 × 14 mm		
Space between two layers of elements = 1 cm		
Elements thickness = 0.5 mm		

Figure 5. Flexible roughness element on NACA 4412 tapered wing.

FACILITY AND FORCE BALANCE

All experiments have been carried out in the IIUM low speed closed loop wind tunnel located in the Mechanical Engineering Department of International Islamic University of Malaysia, which has a test section of 2.3 × 1.5 × 6 m with optically transparent walls. The maximum airspeed in the wind tunnel is 50 m/s and the turbulence intensity of flow is < 0.11%. Tests were performed at a free stream speed from 20 m/s. A six-component balance was used to measure the forces and moments. The half model normal force has a measurement range of ±2000 N and the uncertainty of 0.0406% FS. The axial force has a measurement range of ±700 N and the uncertainty of 0.04975% FS. The pitching moment has a measurement range of ±250 N.m and the uncertainty of 0.04143% FS. The maximum blockage ratio is 4.7%, which is less than 5%. Figure 6 shows a NACA 4412 half-span taper wing installed in the IIUM wind tunnel.
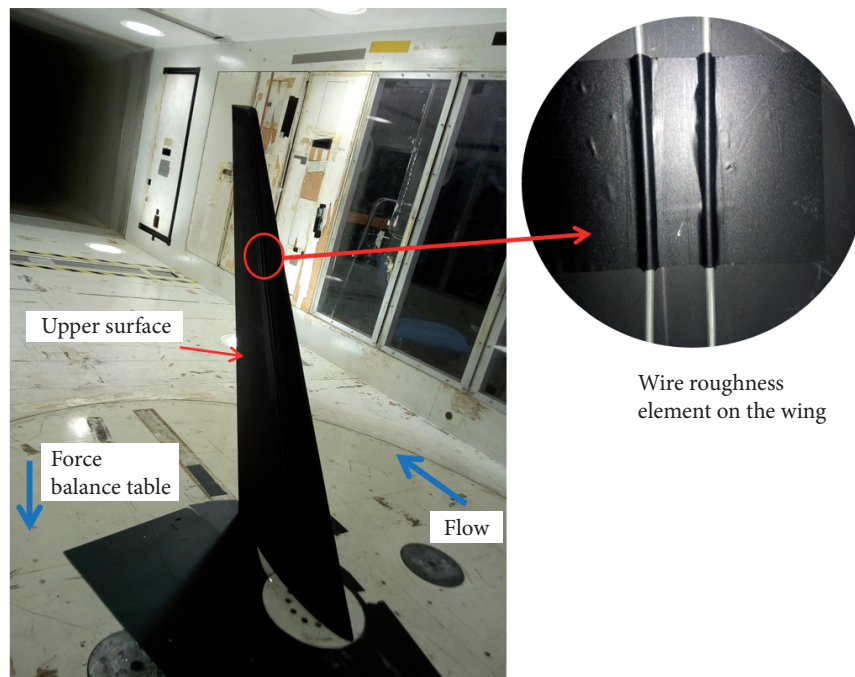
Figure 6. Roughness element (CRE7) and wing arrangement-IIUM wind tunnel.

RESULTS AND DISCUSSION

In this section results and general observation will be discussed, most importantly, maximum lift coefficient, drag and L/D ratio. The discussion will follow with a detailed analysis of Lift, drag, L/D ratio and pitching moment. Each one will be considered with a discussion of the effect on surface roughness.

LIFT

The lift coefficient is calculated from $L/q\infty S$, where S is the base wing planform area. Figure 7 shows the variation of lift coefficient (C_L) with angle of attack (α). As α increases, the C_L increases gradually until it reaches its maximum value and then the C_L drops at the stalling angle. The base wing (smooth) shows a higher C_L in the region from zero angles of attack up to the stall angle ($\alpha = 14°$) compared to the other models of different roughness elements. The maximum lift coefficient ($C_L$max) of the smooth wing before stalling occurs at $\alpha = 14°$ with a $C_L$max of 0.9668, which indicates the beginning of the stall region. The smooth wing shows lower C_L in the region from zero angle of attack up to the stall angle ($\alpha = -20°$) compared to roughness elements with a minimum lift coefficient ($C_L$min) of –0.5944.

As shown Fig. 7a, CRE1, CRE2, and CRE3 roughness elements for various locations (A, B and C), the lower C_L can be seen in the region for angle of attack from $\alpha = -5°$ to 30° and are slight higher for angle of attack from $\alpha = -5°$ to –30°, compared to smooth wing. The $C_L$max values found were 0.9197, 0.9347, and 0.9454 at 16° angle of attack, which was less than smooth wing. The stall angle was delayed by 2°. Higher value of C_L was found for CRE3 compared to CRE1 and CRE2.

Figure 7b shows C_L variation for CRE4, CRE5, and CRE6 for different locations (A, B and C). Smooth wing has a higher C_L value compared to these roughness elements. The stall angle was delayed by 4° for CRE4 and CRE5 cases at 18°. There was no stall angle change for the CRE6 case. The highest lift coefficients are 0.9274, 0.94, and 0.9509 for CRE4, CRE5, and CRE6, respectively.

The variation of C_L for CRE7, CRE8, and CRE9 cases is shown in Fig. 8a. The stall angle was delayed by 2° for CRE7, CRE8, and CRE9 cases. The maximum lift coefficients were found around 0.9408, 0.9311 and 0.9409 at 16° angle of attack for CRE7, CRE8 and CRE9 rigid roughness elements.
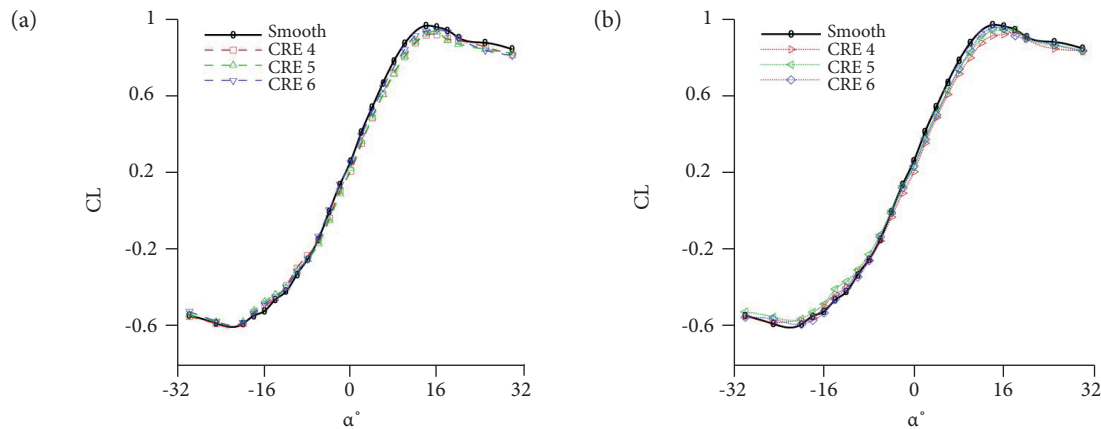
Figure 7. (a) Effect of rigid 0.5 mm size CREs on lift coefficient; (b) effect of rigid 1 mm size CREs on lift coefficient
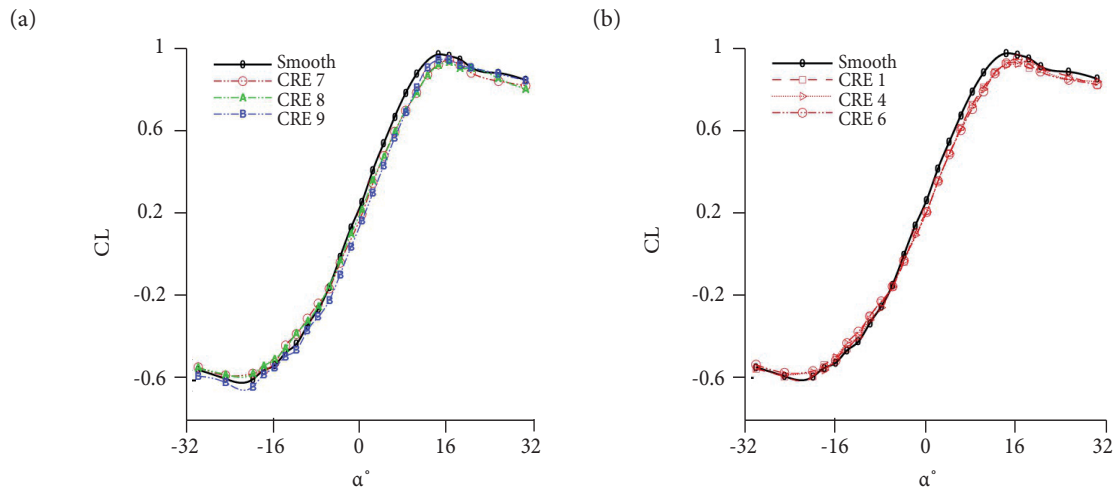

Figure 8. (a) Effect of rigid 2 mm size CREs on lift coefficient; (b) effect of different CREs on lift coefficient at location A.

Figures 8b, 9a and 9b show the effect of different of types of CREs (0.5, 1 and 2 mm diameter) on lift coefficient for locations A, B and C. When sizes of wire roughness elements increase, lift coefficient decreases at location A. A slight decrement in lift coefficient is also observed at locations B and C when wire's size was increased from 0.5 mm to 1 mm.

As shown in Fig. 10a, for the wing with roughness element SRE4, C_L max before stalling occurs at $\alpha = 16°$, is 0.964. After the stall angle of SRE4 case, the C_L is higher than the base wing. For SRE2 roughness element, although lift coefficient is lower than the base wing in the region from zero to stalling angle, the C_L max before stalling begins at $\alpha = 18°$ with a C_L max of 0.9522. Lift coefficient is higher than the base wing for the region $\alpha = -5°$ to $\alpha = -30°$. The SRE1 roughness element produces the lowest C_L in the region from zero angles of attack to $\alpha = 18°$. The highest C_L in the region from $\alpha = -8°$ to $\alpha = -30°$ is due to SRE1 roughness model. The C_L max observed 0.9522 at $\alpha = 18°$ for roughness element SRE1. There was no significant effect observed on lift coefficients using roughness element SRE3, it always lies near smooth wing lift. The highest value of C_L found is around 0.9383 at $\alpha = 18°$. The stall angle is delayed by 2° for SRE4 and by 4° for roughness elements SRE1, SRE2 and SRE3.

The effect of triangular type of roughness wing element is shown in Fig. 10a. TRE shows the decrease in lift coefficients at $\alpha = 0°$ to $\alpha = 16°$. In the region from $\alpha = -5°$ to $\alpha = -30°$, lift curve follows the smooth's lift, which indicates no notable change in lift coefficients. The C_L max is 0.9401 at $\alpha = 16°$ angle of attack. The stall angle is found to be delayed by 2° for this roughness element.
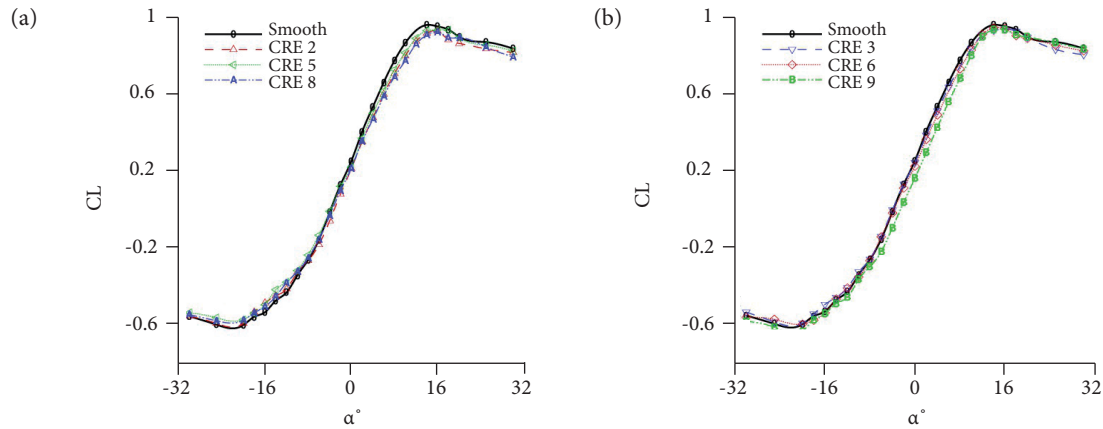
Figure 9. (a) Effect of different CREs sizes on lift coefficient at location B;
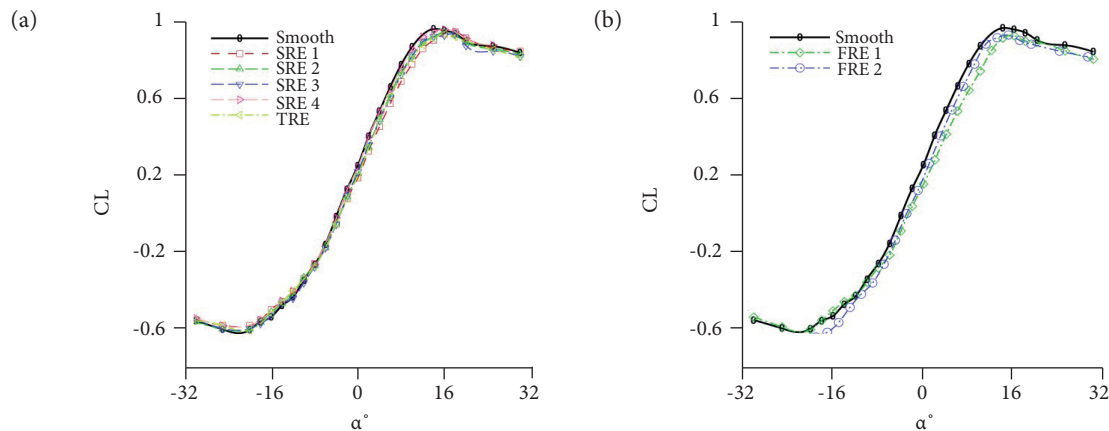(b) effect of different CREs sizes on lift coefficient at location C.

Figure 10. (a) Effect of SREs & TRE on Lift coefficients; (b) effect of FREs on lift coefficient.

As shown in Fig. 10b, in case flexible roughness element FRE1, the decrease in C_L occurs at α = −12° to α = 30°, the rest of angles of attack do not show any change in C_L compared to base model. The $C_L$max at stalling angle is 0.9268. For FRE2 case, flow begins to stall at α = 15°, which is delayed by 1° when it reaches its maximum value of 0.9303. A lower C_L is observed compared to smooth wing for both elements.

For SRE4, TRE, CRE1, CRE2, CRE3, CRE7, CRE8, CRE9, FRE1, and FRE2 roughness element cases, the $C_L$max and stall occurs at angle of attack α = 16° with $C_L$max of 0.964, 0.9401, 0.9197, 0.9347, 0.9454, 0.9409, 0.9311, 0.9409, 0.9268, and 0.9303, respectively. So, the stalling angle is delayed by 2° compared to the smooth wing. For roughness elements SRE1, SRE2, SRE3, CRE4 and CRE5, $C_L$max occurs at angle of attack (α = 18°), with $C_L$max of 0.9522, 0.9558, 0.9383, 0.9274 and 0.94, respectively, and the stall angle is delayed by 4° compared to the smooth wing. For CRE6 roughness element, $C_L$max found at angle of attack α = 14°. There was no delay observed in the stall angle.

For comparison, no increment in C_L was reported after applying bump on the surface near the leading edge of an airfoil, although they studied only for angle of attack 2°, 4° and 6° (Zhou and Wang 2011). Chakroun *el al.* (2004) and Zhou and Wang (2011) reported the value of stall angle delayed by 4° for wire roughness (2 mm size wire) element on wing located at LE. For location at trailing edge, a 2° delay in stall angle and highest C_L up to stall angle was reported. The lowest C_L was reported when

the roughness element is located at the leading edge (Chakroun *et al.* 2004). Xia *el al.* (2014) reported lower C_L than smooth airfoil from 0° to 10° and higher C_L than smooth airfoil for 0° to –10° angle of attack. Chen *et al.* (2016) found that C_L drops by around 40% compared to smooth when size of roughness elements rises from 0.2 mm to 1.5 mm. The effect on C_L was higher when roughness elements are placed at 10% of the chord from the leading edge compared to near trailing edge location. Van Bokhorst *et al.* (2015) reported limited effect on C_L for rough model compared to smooth model at Reynolds number from 15,000 to 30,000.

DRAG

The drag coefficient (C_D) variation versus angle of attack for different roughness elements is shown in Fig. 11. The minimum drag coefficient ($C_D$min) is observed at zero angles of attack for all wing models. It is seen that, as the angle of attack increases, the C_D also increases gradually until it reaches its maximum value at the maximum angle of attack. The C_D at a high angle of attack occurred due to the separation of the stream flow from the upper surface of the wing, due to the high positive pressure gradient. As the angle of attack increases, the pressure gradient also increases and hence the separation point moves towards the leading edge, causes larger separation region and hence larger drag.

As shown in Fig. 11a, the minimum value of drag coefficient ($C_D$min) for the smooth wing is found to be around 0.011. The drag coefficient of wing with wire roughness elements for 0.5 mm size (for CRE1, CRE2 and CRE3), 1 mm size (for CRE4, CRE5 and CRE6), and 2 mm size (for CRE7, CRE8 and CRE9), increases for all angle of attack as compared to the smooth wing. For CRE1, CRE2 and CRE3, the $C_D$min is slightly higher than the $C_D$min for the smooth wing for all positive and negative angles of attack. The value of $C_D$min at zero angles of attack is 0.0191, 0.0239 and 0.0169, compared to the smooth wing element, there is an increase in minimum drag coefficient of 73.9%, 115.3%, and 52.3%. The $C_D$min for CRE4, CRE5 and CRE5, are 0.0228, 0.0252, and 0.0196, respectively; therefore, $C_D$min is increased by 105.4%, 127%, and 76.6%, respectively. For CRE7, CRE8 and CRE9, the $C_D$min are 0.0222, 0.0244 and 0.022, respectively; therefore, $C_D$min is increased by 100 %, 119.8%, and 98.2%, respectively.

As shown in Figs. 11b, 12a and 12b, the cylindrical roughness elements, which show the highest $C_D$min, were selected for further examination to study the surface roughness effect of different sizes by varying the location for analyzing aerodynamic characteristics. As shown in Fig. 12b, the cases where the CRE3, CRE6 and CRE9 are located at C, show lower drag coefficients as compared to those at locations A and B. As shown Fig. 12a, CRE2, CRE5 and CRE8 located at B, show higher drag coefficients as compared to that of location C. The same roughness effect on drag coefficient are reported by (Chakroun *et al.* 2004). Based on the obtained results, roughness at locations A and B show higher drag coefficients compared to location C. So, roughness at these locations should be avoided. In the 2 and 1 mm wire sizes for B location cases, higher C_D is found. This location is very sensitive for C_D.
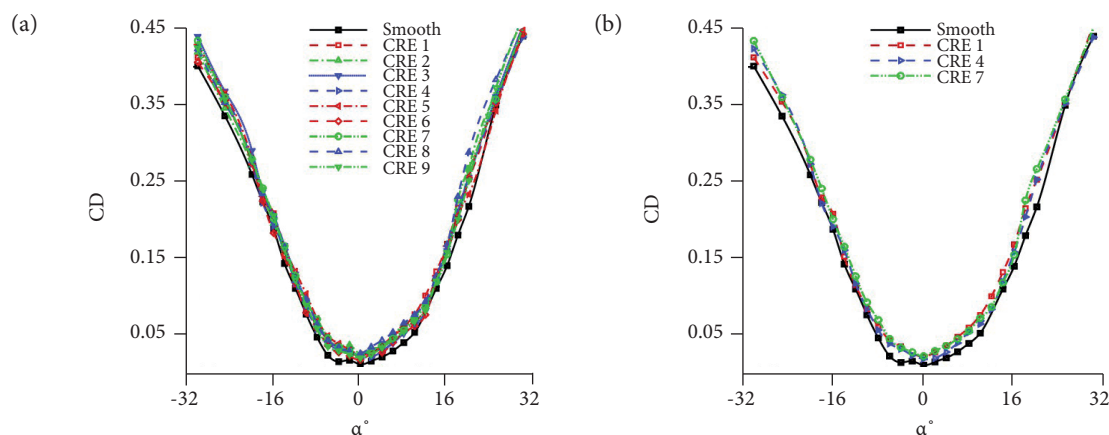

Figure 11. (a) Effect of rigid cylindrical roughness on drag coefficient; (b) effect of rigid cylindrical roughness size on drag coefficient at location A.

Figure 13a shows the $C_D$min for SRE1, SRE2, SRE3, and SRE4 are found to be around 0.015, 0.015, 0.014, and 0.011, respectively; therefore, $C_D$min for SRE1, SRE2, SRE3, and SRE4 roughness elements is increased by 37%, 31%, 25% and 2%, respectively. For TRE roughness cases, the $C_D$min value is 0.0142, which has an increment of 28% compared to smooth. In cases of FRE1 and FRE2, the $C_D$min is 0.0279 and 0.0183 at zero angles of attack (see Fig. 13b), which shows a 151.4% and 64% rise in the $C_D$min compared to smooth wing element.

Based on the obtained results, roughness element SRE1 shows the highest value of $C_D$min by 37% increment compared to the square types of roughness elements. In cylindrical roughness element cases, CRE5 and CRE8 showed highest $C_D$min 127% and 120% increment. The FRE1 shows the highest $C_D$min, 151% increment compared to FRE flexible roughness element. So, these roughness wing models should be avoided. The lowest $C_D$min value is the one of SRE4 roughness by 1.8% increment. At larger angles of attack, the difference in the C_D due to roughness size is small. In this interval, the C_D due to pressure gradient on the upper surface is dominant. So, the separation point will move towards the leading edge and therefore the effect of surface roughness is almost negligible. Chakroun *et al.* (2004) stated that the reason for increment in the $C_D$min with the increment of roughness size is the increase in the viscous stresses developed within the boundary layer, which leads to a higher skin friction.
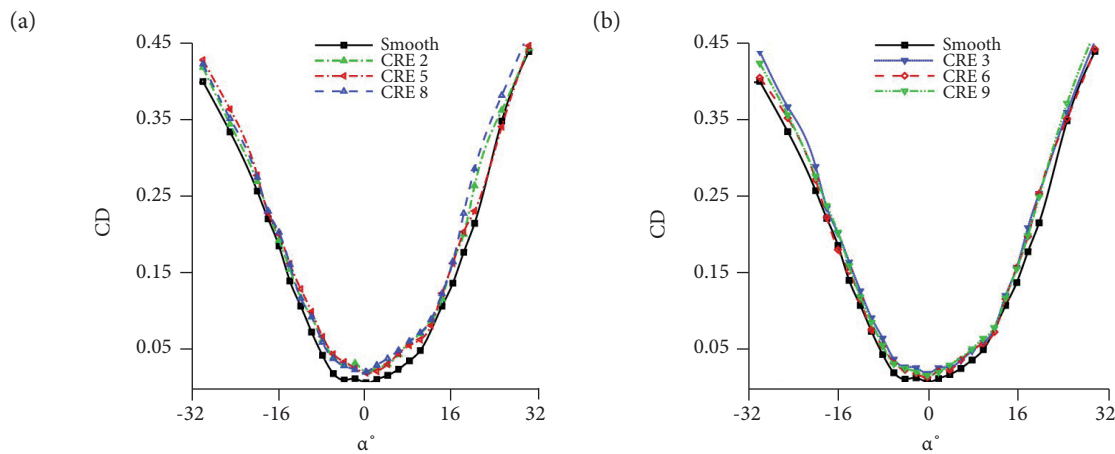

Figure 12. (a) Effect of rigid cylindrical sizes on drag coefficient at location B;
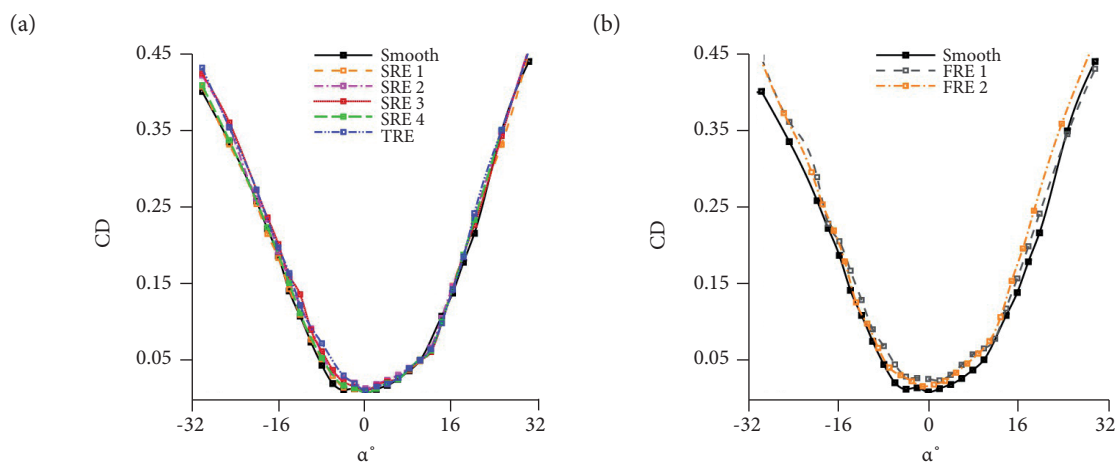(b) effect of rigid cylindrical sizes on drag coefficient at location c.

Figure 13. (a) Effect of rigid square and triangular roughness on drag coefficient;
(b) effect of flexible roughness on drag coefficient.

That is why the wing with the 2 mm wire (cylindrical) size rough element has the highest $C_D$min value of 0.024 at B location compared to the 0.5 and 1mm.

For comparison, Zhou and Wang (2011) reported, after applying bump on the surface, that C_D decreased compared to smooth model when bump surface was placed near leading edge of SD7003 rectangular wing at 60,000 Reynolds number. On the other hand, van Bokhorst *et al.* (2015) reported that the effect of rough surface on C_D is very week compared to smooth Swift bird wing model for low Reynolds numbers from 15,000 to 30,000. Chen *et al.* (2016) reported that C_D increases when roughness elements are applied to smooth airfoil for a Reynolds number of 0.4×10^6.

The drag coefficient increases when roughness element is applied on smooth airfoil surface. Increment in drag for rough surface airfoil compared to the smooth surface at higher Reynolds number (more than 24000), are also reported by Chakroun *et al.* (2004), Chen *et al.* (2016), Lentink and Kat (2014), Murphy and Hu (2010), van Bokhorst *et al.* (2015) and Xia *et al.* (2014).

LIFT-TO-DRAG RATIO (L/D)

Lift to drag ratio (L/D) is one of the most important parameters affecting wing aerodynamic performance. The lift to drag ratio curve gives the optimum value of α for different wings. As shown in Fig. 14, the smooth wing shows the highest lift to drag ratio, (L/D)max, smooth = 26.85 at an angle of attack 2°.

Figure 14a shows L/D ratio for cylindrical roughness elements CRE1, CRE2, CRE3, CRE4, CRE5, CRE6, CRE7, CRE8 and CRE9. It shows a lower lift to drag ratio compared to the smooth wing element, (L/D)max = 17.22, 13.84, 19.63, 13.36, 11.97, 15.57, 13.17, 13.63 and 14.59 at an angle of attack 2°, 4°, 4°, 6°, 4°, 2°, 4°, 4° and 6°, respectively.
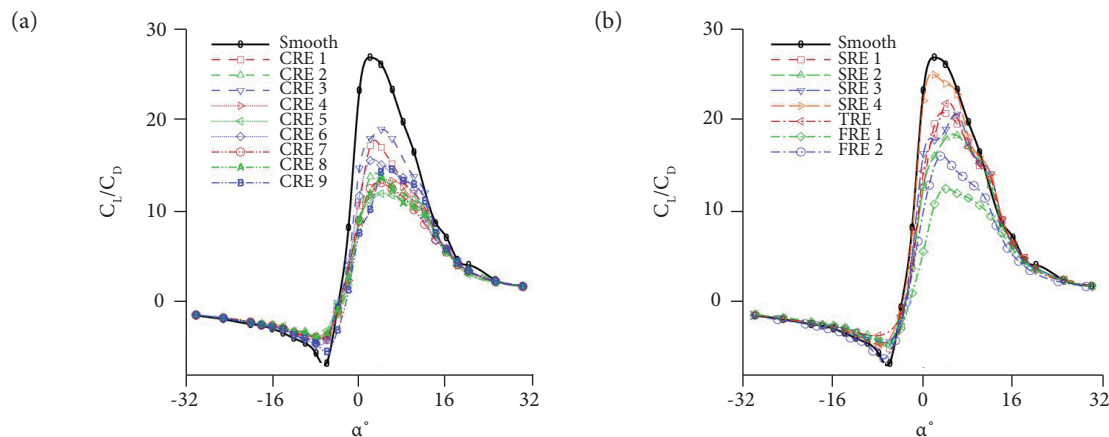

Figure 14. (a) Effect rigid CREs on variation of L/D; (b) effect rigid SREs, TRE and FREs on variation of L/D.

As shown in Fig. 14b, the roughness elements SRE1, SRE2, SRE3, SRE4, TRT, FRE1 and FRE2 cases show a lower lift to drag ratio compared to the smooth wing element, (L/D)max = 20.72, 23.76, 20.68, 24.97, 21.82 12.5 and 16.08 at an angle of attack 4°, 4°, 6°, 2°, 4°, 4° and 3°.

For comparison, it was reported by Chakroun *et al.* (2004) that the lift to drag ratio is lower for a rough airfoil compared to an airfoil with a smooth surface. Xia *et al.* (2014) found lower lift to drag ratio of rough airfoil compared to a smooth one. Chen *et al.* (2016) reported that L/D ratio declines after applying roughness elements on a smooth airfoil. In contrast, Zhou and Wang (2011) reported 3%, 13% and 19% increment in L/D ratio after applying bump at leading edge of a SD7003 rectangular wing for angle of attack 2°, 4° and 6°. Van Bokhorst *et al.* (2015) found limited effect of roughness on L/D ratio compared to smooth one.

There was decrease in lift coefficient due to roughness elements on wing surface, CRE5 displays lowest L/D ratio by a decrement of approximately 55%. The highest L/D ratio is obtained for SRE4 with a 7% decrement compared to all roughness element cases. Therefore, the smooth wing is the most efficient wing compared to other roughened wings. As the roughness size increases, the

efficiency of the wing decreases. For better aerodynamic performance at moderate to high Reynolds numbers, surface roughness must be avoided in general. Improvement in aerodynamic performance at low Reynolds number (up to 24,000) is reported by (Lentink and de Kat 2014; Lentink *et al.* 2007; van Bokhorst *et al.* 2015).

PITCHING MOMENT

Perhaps no data has been reported in the open literature on the effect of roughness elements on the pitching moment of a wing or an airfoil.

Figures 15a and 15b show variation in the pitching moment coefficient ($C_{Mc/4}$) for all tested wing models. The $C_{Mc/4}$ values range from –0.8 to +0.6 in all cases. From angle of attack –30° to –8° the $C_{Mc/4}$ drops steadily. Followed by a drastic decline of moment slope until an angle of attack 10° from positive to negative values. The $C_{Mc/4}$ decreases as the angle of attack increases gradually until angle of attack α = 12° to 16°, and after this region it becomes approximately steady. The $C_{Mc/4}$ increases as angle of attack decreases gradually in region from α = –6° to –30°. This negative slope shows a longitudinal stability in this range. Then from angle of attack 10° to 24°, it shows a slightly positive slope. There is a slight variation in the pitching moment slope in the range 24° to 32°.
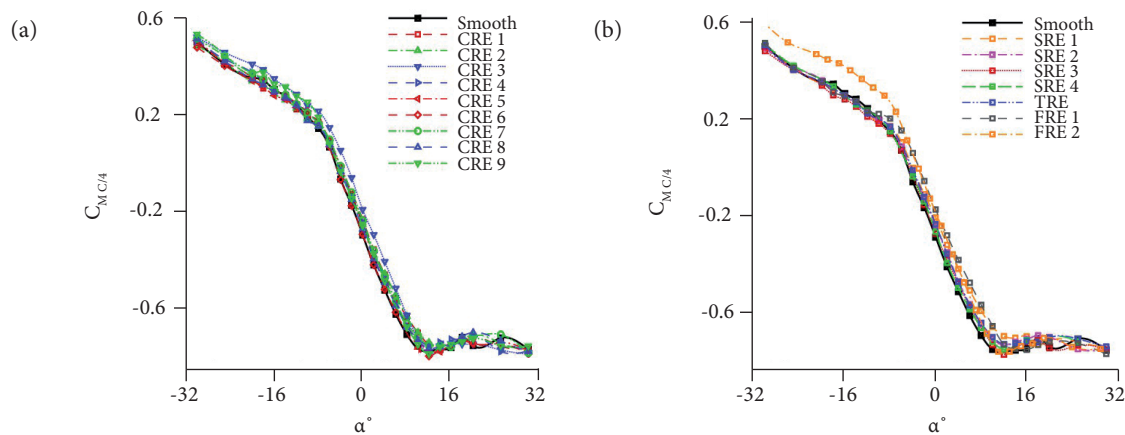

Figure 15. (a) Effect rigid CREs on pitching moment coefficient;
(b) effect rigid SREs, TRE and FREs on pitching moment coefficient.

The $C_{Mc/4}$ graph results for all rigid roughness elements suggest that there is a small increment in the magnitude of the pitching moment as compared to the clean smooth wing. The slopes do not change. SRE1 and CRE9 roughness elements show higher $C_{Mc/4}$ compared to the other tested roughness elements. The effect of surface roughness element CRE3 on $C_{Mc/4}$ curve shows the smallest effect compared to the other elements. A negative value of $C_{Mc/4}$ at zero angle of attack is observed for all tested elements.

The major effect of roughness over $C_{Mc/4}$ can be seen in cases of flexible roughness element (FRE1). As shown in Fig. 15b, $C_{Mc/4}$ for FRE1 and FRE2 flexible roughness elements lies significantly higher than smooth wing, especially at larger negative angles of attack.

CONCLUSIONS

Wind tunnel tests were conducted to examine aerodynamic properties of different sized roughness elements over a NACA 4412 half-span tapered swept wing with a sweep angle of 30° and a dihedral angle of 5°. The investigations were performed at a Reynolds number 4×10^5 for angles of attack ranging from –30° to 30°. C_L, C_D, and $C_{Mc/4}$ were acquired and compared to both clean and rough surface wings to examine the effect of different types of roughness elements on aerodynamic properties. The lift coefficient decreases, and minimum drag coefficient increases as size of roughness surface increases. Stall angle is delayed by roughness

elements and the maximum delay was between 2° to 4°, compared to the smooth wing. In addition, the maximum influence of roughness elements was detected at the 50% to 70% of mean chord from leading edge, which shows higher minimum drag and lower lift for rigid rough elements. For the location 75% to 95% of mean chord from leading edge, rough models showed higher lift (up to the stall angle) compared to the other cases. The L/D ratio is highest for the smooth wing, compared to any other wing with roughness elements. Therefore, the smooth wing is the most efficient element compared to the other roughened elements. As the roughness size increases, the efficiency of the wing decreases.

Furthermore, the magnitude of pitching moment coefficient rises after applying a roughness element. The pitching moment coefficient increases significantly when flexible surface roughness elements are used, compared to the rigid roughness elements.

AUTHOR'S CONTRIBUTION

Conceptualization, Asrar W, Erwin S and Malik K; Methodology, Malik K, Asrar W and Aldheeb M; Investigation, Malik K, Aldheeb M, Asrar W and Erwin S; Writing – Original Draft, Malik K; Writing – Review and Editing, Asrar W and Malik M.

FUNDING

REFERENCES

Bartenwerfer M, Bechert D (1991) Viscous flow on hairy surfaces. Zeitschrift fuer Flugwissenschaften und Weltraumforschung 15:19-26.

Bechert D, Bruse M, Hage W, Meyer R (2000) Fluid mechanics of biological surfaces and their technological application. Naturwissenschaften 87(4):157-171. https://doi.org/10.1007/s001140050696

Carruthers AC, Walker SM, Thomas ALR, Taylor GK (2010) Aerodynamics of aerofoil sections measured on a free-flying bird. Proceedings of the Institution of Mechanical Engineers, Part G: Journal of Aerospace Engineering 224(8):855-864. https://doi.org/10.1243/09544100jaero737

Chakroun W, Al-Mesri I, Al-Fahad S (2004) Effect of surface roughness on the aerodynamic characteristics of a symmetrical airfoil. Wind Engineering 28(5):547-564. https://doi.org/10.1260/0309524043028136

Chen J, Xie S, Li H, Luo J, Zhao C (2016) Roughness effect on airfoil aerodynamic performance for land-yacht robot. Journal of Renewable and Sustainable Energy 8:025701. https://doi.org/10.1063/1.4941794

Crandell KE, Tobalske BW (2011) Aerodynamics of tip-reversal upstroke in a revolving pigeon wing. Journal of Experimental Biology 214:1867-1873. https://doi.org/10.1242/jeb.051342

Ennos A, Hickson J, Roberts A (1995) Functional morphology of the vanes of the flight feathers of the pigeon Columba livia. Journal of Experimental Biology 198:1219-1228.

Gregory N, O'Reilly C (1973) Low-Speed aerodynamic characteristics of NACA 0012 aerofoil section, including the effects of upper-surface roughness simulating hoar frost. (Reports and Memoranda No 3726). HM Stationery Office.

Hope Rutledge (2018) American Bald Eagle Information; [accessed 2018 January 5]. www.baldeagleinfo.com

Jakab PL (1990) Visions of a flying machine. Washington: Smithsonian Institution Press.

Klän S, Bachmann T, Klaas M, Wagner H, Schröder W (2009) Experimental analysis of the flow field over a novel owl based airfoil. Experiments in Fluids 46(5):975-989. https://doi.org/10.1007/s00348-008-0600-7

Laursen L (2008) Robot fliers in commando competition. Nature International Weekly Journal of Science; [accessed 2017 October 02]. https://doi.org/10.1038/news.2008.659

Lentink D, de Kat R (2014) Gliding swifts attain laminar flow over rough wings. PloS ONE 9(6):e99901. https://doi.org/10.1371/journal.pone.0099901

Lentink D, Müller UK, Stamhuis EJ, de Kat R, van Gestel W, Veldhuis LL, Henningsson P, Hedenström A, Videler JJ, van Leeuwen JL (2007) How swifts control their glide performance with morphing wings. Nature 446:1082-1085. https://doi.org/10.1038/nature05733

Murphy JT, Hu H (2010) An experimental study of a bio-inspired corrugated airfoil for micro air vehicle applications. Experiments in Fluids 49(2):531-546. https://doi.org/10.1007/s00348-010-0826-z

Schlichting H, Gersten K, Krause E, Oertel H (1955) Boundary-layer theory. Berlin: Springer. https://doi.org/10.1007/978-3-662-52919-5

Shyy W, Aono H, Kang C-K, Liu H (2013) An introduction to flapping wing aerodynamics. New York: Cambridge University Press.

van Bokhorst E, de Kat R, Elsinga GE, Lentink D (2015) Feather roughness reduces flow separation during low Reynolds number glides of swifts. Journal of Experimental Biology 218:3179-3191. https://doi.org/10.1242/jeb.121426

White FM, Corfield I (1991) Viscous fluid flow. New York: McGraw-Hill.

Withers PC (1981) An aerodynamic analysis of bird wings as fixed aerofoils. Journal of Experimental Biology 90:143-162.

Xia Y, Bilgen O, Friswell MI (2014) The effect of corrugated skins on aerodynamic performance. Journal of Intelligent Material Systems and Structures 25(7):786-794. https://doi.org/10.1177/1045389x14521874

Zhou Y, Wang Z (2011). Effect of surface roughness on laminar separation bubble over a wing at a low-Reynolds number. Presented at: 49th AIAA Aerospace Sciences Meeting; Orlando, USA. https://doi.org/10.2514/6.2011-73